Chapter 7
Thermal and Mechanical Properties (I): Optimum Predictive Thermal Conduction Model Development for Epoxy-Filled Copper Oxide Nanoparticles Composite Coatings on Spent Nuclear Fuel Steel Casks

Daniel Ogochukwu Okanigbe and Shade Rouxzeta Van Der Merwe

7.1 Introduction

Nuclear reactors use radioactive elements to generate power [1, 2]. While the by-product of generating energy from radioactive materials is known as spent nuclear fuels (SNF) [3, 4], it is anticipated that this waste will be safely stored and disposed of following conditioning and treatment [5–7]. Consequently, one of the biggest issues facing the nuclear industry is SNF management [8, 9]. All transportation casks are anticipated to be built to comply with radiation safety regulations as part of managing SNF [10–12].

Therefore, type B casks (Fig. 7.1) are used to transport SNF assemblies in order to comply with requirements that restrict radiation leaks and doses that represent a risk to the general public's health and safety as well as the environment [13–16]. The casks are made of steel (or a steel and lead alloy) and are shielded [17–19]. The steel is typically around 30 cm thick and protects the fuel element while shielding the casks from radiation.

It has been discovered that the deposition of radioactive salts during spent fuel transportation frequently results in high-radiation levels in casks. The technique of

D. O. Okanigbe (✉)
Department of Chemical, Metallurgical and Materials Engineering, Faculty of Engineering and the Built Environment, Tshwane University of Technology, Pretoria, South Africa

Pantheon Virtual Engineering Solutions, Nigel, South Africa
e-mail: okanigbedo@tut.ac.za; okanigbeogochukwu@gmail.com

S. R. Van Der Merwe
Department of Mechanical and Mechatronics Engineering, Faculty of Engineering and the Built Environment, Tshwane University of Technology, Pretoria, South Africa
e-mail: vandermerweR1@tut.ac.za

D. O. Okanigbe, A. P. Popoola (eds.), *Resource Recovery and Recycling from Waste Metal Dust*, https://doi.org/10.1007/978-3-031-22492-8_7

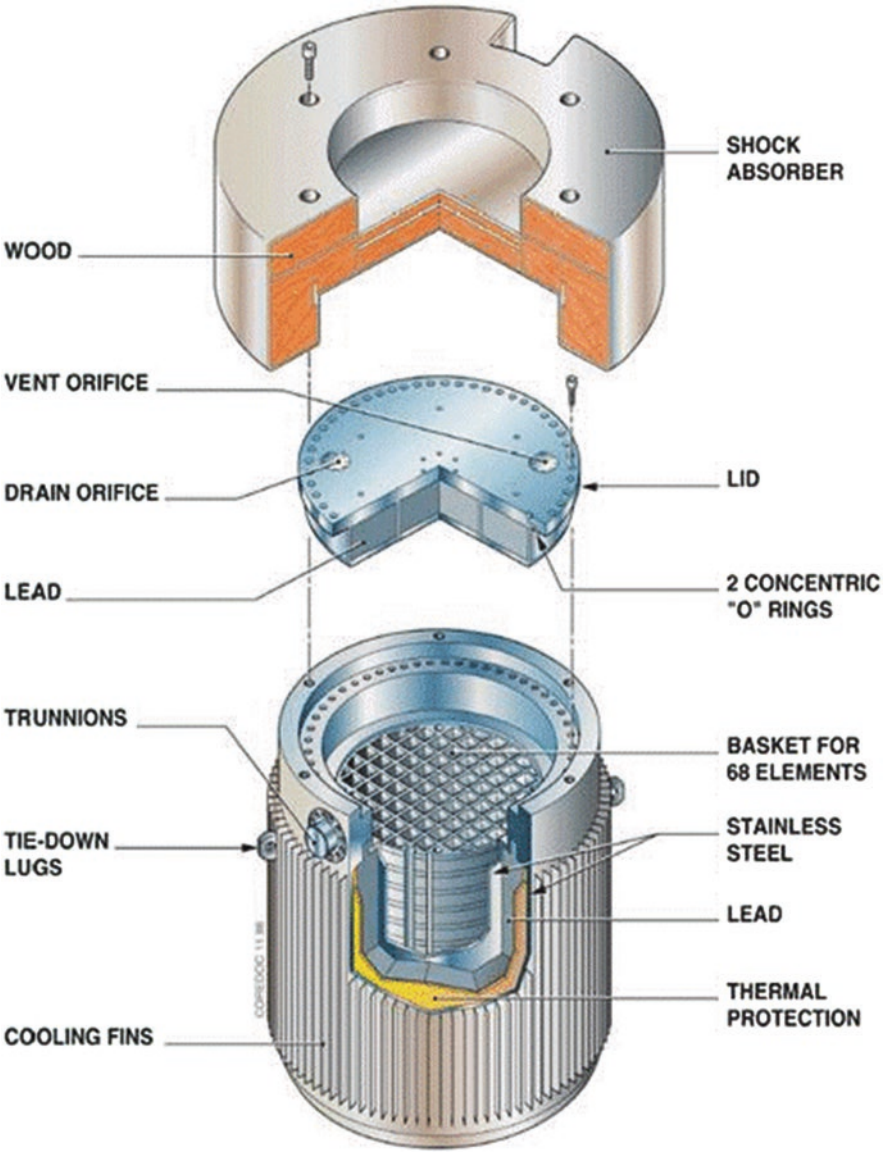

Fig. 7.1 A typical type B SNF transportation cask. (Source: Google image)

eliminating these salts involves sanding, which involves directing an airstream filled with sand toward areas where they have gathered and there is a lot of radiation since this causes mechanical corrosion in those areas [20].

In accordance with Shkoukani Al-Qous [21], steel is exposed to radiation both internally and externally. As a result, the cumulative gamma irradiation effect on steel corrosion behavior results in a rise in corrosion rate with increasing irradiation dose.

As was previously indicated, the corrosion of the steel used to protect the casks (Fig. 7.1) can cause significant economic losses as well as potential safety issues [22]. Surface coating has frequently been employed to protect the steel casks from mechanical and biological corrosion in order to alleviate these issues. However, surface coatings have a low resistance to electrolyte diffusion, which prevents them from offering long-term protection against corrosion [23]. As a result, numerous recent studies have been carried out to enhance these coatings' anticorrosion abilities [20, 24, 25].

Tensile stress, a corrosive environment, and a susceptible material are the three prerequisites for corrosion of steel casks, according to Ross et al. [26]. When assessing corrosion susceptibility, it is important to comprehend and take these circumstances into account. The three criteria will eventually be met in dry storage of SNF, according to previous studies [27–35].

Knight et al. [16] emphasized the significance of a material that is vulnerable to corrosion. The majority of SNF canisters is constructed of 304 stainless steel, which means that weld residual tensile stresses are adequate for corrosion to occur and that a corrosive environment has the potential to develop, according to the researchers. The presence of a chloride-rich brine on the surface of SNF canisters poses the greatest risk for corrosion [36–46].

By reducing or completely eliminating the interaction of a corrosive brine with the canister surface, the researchers continued to emphasize the significance of surface coating materials in the prevention, mitigation, and repair potential of corrosion. By separating the metal surface from the corrosive environment on the coated canister surface, an efficient coating would do away with the chance of corrosion. By acting as a physical barrier that restricts mass transfer to the metal substrate, the majority of coatings either isolate the metal surface from exposure to aggressive chemistry or prevent corrosion by using corrosion inhibitors, such as organic inhibitors (i.e., organic coatings). Organic inhibitors protect the metal by forming a hydrophobic film on the metal surface. The chemical make-up, molecular structure, and surface affinities of this class of inhibitors all affect how effective they are.

These anticorrosion coatings must, however, have excellent thermal conductivity properties as prescribed by the energy application (i.e., steel cask for transportation of SNF). A composite made of thermally conductive nano- or micro-sized particles spread in a polymer matrix is therefore one of the most efficient ways to create a thermally functional layer [47–51]. In terms of cost and mass production, copper oxide (CuO), which is dark and has a high emissivity of more than 0.9, stands out among these materials and is a potential option for altering the metal heat sink surface to enhance heat dissipation in passive cooling [52].

By creating nanocomposite coatings and adding inorganic nano-fillers to the coating composition, the characteristics of organic coatings can be further enhanced [53]. The most often utilized inorganic nano-sized reinforcing fillers include carbon nanotubes, copper, zinc, titanium, magnesium, and gold [54, 55]. In terms of thermal stability, mechanical, electrical, and catalytic capabilities, these hybrid coatings are discovered to be superior. The enhancement of these properties is due to the robust interfacial interaction between the polymer and the inorganic components,

which results from the substantial specific surface area of the nano-sized inorganic components [56]. However, to create hybrid materials with desired qualities, a homogenous dispersion of the inorganic fillers must be attained inside the polymer matrix [57].

Additionally, because the contact between the coating layer and the metal surface depends on mechanical interlocking, bonding that is not at the atomic or molecular level, showing high-interfacial thermal resistance, and as an example, polymer/ceramic composite coating significantly increases the interfacial thermal resistance on the metal surface [58–62].

Up until this point, numerous researchers have created a variety of thermally conductive polymers and their composites using filled type [63]. The thermal conductivity coefficient (λ) values of these polymers and their composites fall short of expectations, which has become the main bottleneck for their energy applications.

Due to this, several types of copper oxide nanoparticles (CuO-NPs) will be produced in the proposed study from concentrates acquired during the density separation of waste copper dust (WCD), depending on their copper oxide, aluminum oxide, and silicon oxide contents [64]. This class of organic–inorganic composite coating will be studied to better understand the phenomenon of interfacial thermal resistance, an understanding that should assist with improving the coating's performance when used as a surface coating on steel casks during the transportation of SNF [65, 66]. These various compositions of CuO-NPs will be used to create an epoxy/CuO-NPs composite coating.

7.2 Problem Statement

The following basic discussions pertain to steel containers used to transport SNF and its surface coating:

1. Despite the enormous research efforts, there are still problems with the current hydrophobic coating methods, including poor mechanical strength and limited durability [54].
2. Despite numerous attempts to prepare a variety of thermally conductive epoxy composites using filler type [67], these epoxy composites frequently struggle to meet expectations in terms of their thermal conductivity coefficient values, which restrict their use in energy applications [68].
3. Epoxy composites with a higher filler content display deposition and agglomeration in the polymer matrix, which leads to poor adhesion between the filler particles and epoxy resin and reduced mechanical strength and durability [69].

7.3 Research Objectives

7.3.1 Main Objective

Investigating the interfacial thermal resistance and anticorrosion performance of CuO-NPs-Epoxy composite coatings from WMD on SNF steel casks is the main objective of this study.

7.3.2 Sub-Objectives

By responding to the following research questions provided as sub-objectives, the main goal will be accomplished:

1. What is WCD's characteristics?
2. What makes up the concentrates and tailings produced by the WCD density separation?
3. What is the makeup of the leach solutions made from the various concentrate compositions?
4. What is the makeup of the copper precursor produced by the chemical reaction between reagents and leach solutions?
5. What makes up the CuO-NPs created by the thermal breakdown of various copper precursors?
6. What is the interfacial thermal resistance of the hybrid nanocomposite coatings made by adding different compositions of CuO-NPs to epoxy resin?
7. What is the anticorrosion behavior of hybrid nanocomposite coatings made by adding various compositions of CuO-NPs to epoxy resin?
8. What are the CuO-NPs/epoxy composite coatings' calculated and predicted thermal conductivity value (λ) for the given system?

7.4 Research Hypotheses

On the basis of the model proposed to overcome the challenges noted, the following can be hypothesized:

1. Decreased thermal resistance between surfaces.
2. Hybrid coatings' improved anticorrosion behavior.
3. Decreased cost of hybrid coating production.
4. Utilization of the earth's mineral resources sustainably.

7.5 Significance of Study

The positive outcome of this research will be advantageous to the following areas:

1. Creation of a hybrid coating that enables the economical design of superb thermally conductive steel containers for the transfer of SNF.
2. The earth's ability to support life despite other deteriorating environmental factors, while also providing WCD as a natural resource replacement for copper-based surface exploration.
3. Using an economical and effective approach of fabrication and processing to create hybrid coatings for steel barrel designs.

7.6 Literature Review

7.6.1 Background and Literature Survey

7.6.1.1 Background

Transportation of SNF

Every year, about 20 million transports of radioactive materials are made worldwide. However, shipping of materials used in the production of electricity make up a very minor portion of all radioactive material shipments made globally. The global transportation of used nuclear fuel has been done safely. No incident or mishap involving the transfer of SNF in the past 45 years has had a substantial radiological effect on either people or the environment. To date, used nuclear fuel has been shipped throughout the globe in excess of 80,000 tons.

Strong international transportation standards that have been approved and implemented by national regulatory programs are directly responsible for the industry's great safety record. According to the laws, radioactive material packages and casks must meet performance standards that are appropriate for the level of risk posed by the substances they are intended to hold. Extra-regulatory testing of radioactive material transportation packages and casks as well as investigations into serious, non-radioactive accident cases have shown that the current regulatory system is effective and that it is safe to transport radioactive materials, including SNF.

In some circumstances, such as transfer to another storage facility or transportation to a central storage location, a cask may need to be transported from one storage location to another storage location. This may be due to economic factors, such as enabling the full decommissioning of the facilities at a reactor site, or political factors such as the political consolidation of storage facilities in a given region or nation.

A cask could occasionally need to be moved from the storage location to the repository. The architecture of the disposal facility and the type of storage

technology to be employed both need to be taken into account. Some storage methods used in the US were based on sealed canisters enclosed in concrete storage casks, with the idea being that the canister would act as a containment boundary in the repository rather than requiring the fuel to be unloaded.

However, if the container design does not completely satisfy the standards for the repository or the geological environment in which the fuel will be stored, repackaging of containers may be necessary. Before being disposed of, the fuel is to be repackaged in multipurpose containers or casks, according to alternative repository designs. This idea will be applied in Germany where casks will be accepted at the Pilot Conditioning Plant. There, the spent fuel will be removed from the storage cask and consolidated before being repackaged into disposal casks for disposal in a subterranean repository.

Types of Casks for Transportation of SNF

To specify safety requirements that offer an adequate level of control over radiological dangers, regulations controlling the packaging of radioactive materials have been devised. The laws utilize a graduated approach to the packing requirements because not all radioactive dangers are equal (radiopharmaceuticals used in medicine do not present the same hazard as an SNF).

The packing of radioactive materials depends on the material's classification before it is transported. Excepted, industrial (Type IP), Type A, Type B, and Type C are the five package categories.

Excepted Packages
Materials exhibiting negligible radiological dangers, such as shipments of radiopharmaceuticals, are covered by excepted packages.

Industrial Packages
Industrial packages (Type IP-1, Type IP-2, and Type IP-3) are intended to hold radioactive materials with low-activity levels or radioactive materials with difficult-to-spread radioactivity. The regulatory specifications for the three types of industrial packages range from meeting the general specifications for all packages (Type IP-1), to being able to withstand conditions that might be anticipated during normal transport (Type IP-3), such as falling from a moving vehicle or being struck by a sharp object. Industrial packages are primarily used for the transportation of radioactive ores, low- and intermediate-level radioactive waste, and unirradiated nuclear fuel.

Type A packages
Type A packages are frequently used for the transportation of small but large amounts of radioactive materials. However, the laws include a cap on how much radionuclides they can have. A variety of tests imitating typical transit conditions are performed on Type A packages. For the purpose of reducing possible dispersal in the case of an accident, packages with liquid contents must meet additional

standards. Radioisotopes used for medical diagnosis and some low- and intermediate-level radioactive waste are typical examples of items delivered in Type A packaging.

Type B packages

Type B packaging is necessary for the transportation of highly radioactive materials, such as radioactive sources used in medical imaging equipment, parts taken from nuclear reactor cores, and SNF (Figs. 7.2 and 7.3). Packaging designated as Type B must be able to withstand extreme accident circumstances without leaking or spilling. The relevant authorities or regulators of each nation where the packages are utilized must certify Type B package designs.

Type C packages

The 1996 revision of the IAEA regulations saw the introduction of Type C packages [70]. They are designed for the air transportation of extremely radioactive materials. This kind of bundle has not yet been created. The packaging design can differ greatly among any of the categories for radioactive materials. For instance, Type B packaging intended for used nuclear fuel are frequently very big and heavy, yet Type B packages intended for radioactive sources utilized in different industrial devices may be tiny enough to fit in a car's trunk.

The standards for packing, with the exception of Type C packages, are essentially irrespective of the mode of transportation, whether it is by road, rail, water, or air.

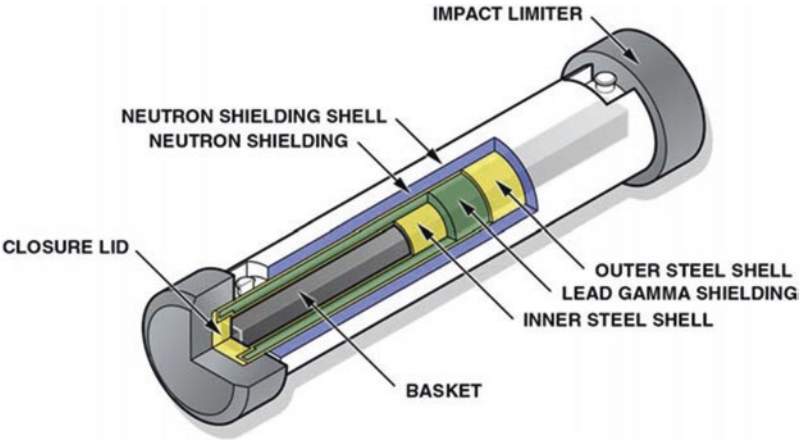

Fig. 7.2 A typical Type B Truck cask for transportation of spent nuclear fuel. (Source: Google image)

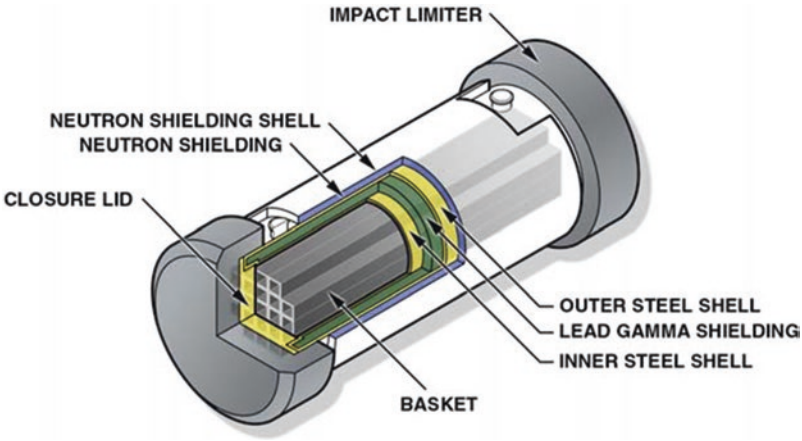

Fig. 7.3 A typical Type B rail cask for transportation of spent nuclear fuel. (Source: Google image)

Steel

In order to increase its strength and fracture resistance compared to other forms of iron, steel used in the production of casks is an alloy composed of iron with typically a few tenths of a percent of carbon. Many additional components could be included or added.

Modern steels are created using various alloy metal combinations to serve a variety of functions. 90% of steel is produced as carbon steel, which is only iron and carbon. To increase the hardenability of thick sections, low-alloy steel is alloyed with additional elements, typically molybdenum, manganese, chromium, or nickel, in amounts up to 10% by weight. In order to boost strength while only slightly raising price, high-strength low-alloy steel incorporates tiny additions (generally 2% by weight) of other elements, often 1.5% manganese.

Steel is susceptible to corrosion, which is caused by electrolysis, in which the metallic surface releases electrons into an electrolyte, such as a layer of moisture in the presence of oxygen. Because metals have a propensity to revert to their original states, this electrochemical reaction takes place.

Therefore, the following techniques are used to prevent corrosion in steel:

1. Store items properly. To considerably slow down rust, store metal products or parts in a low-moisture region or inside a temperature- and humidity-controlled environment.
2. Desiccant drying agents are also useful in this storage.
3. Surface coating, such as galvanizing, which involves dipping metals like iron or steel into a molten Zn metal bath to coat the metal surfaces.

Surface Coatings

Any mixture of film-forming components combined with pigments, solvents, and other additives is referred to as a surface coating. When applied to a surface, this mixture cures or dries to produce a thin film that is both useful and frequently beautiful. Paints, varnishes, enamels, oils, greases, waxes, concrete, lacquers, powder coatings, metal coatings, and fire-retardant formulas are all examples of surface coatings.

According to the composition of their binder, surface coatings are classified as organic or inorganic. Coatings with an organic binder are known as organic coatings. Coatings classified as inorganic contain an inorganic binder, such as a silicate. Surface coating is a method of surface engineering in which the surface of a material is covered with a different material, such as powder, film, or bulk, depending on the desired applications and the coating material.

The following are examples of common coating materials:

1. Pure metals, including Molybdenum (Mo), Copper (Cu), and Aluminum (Al).
2. Alloys like aluminum bronze (CuAl), nickel chrome (NiCr), nickel aluminum (NiAl), etc.
3. Ceramic (Oxide), such as Zirconium Oxide (ZrO_2), Titanium Oxide (TiO_2), Aluminum Oxide (Al_2O_3), etc.
4. Polymers like urethane, silicone, acrylic, phenolic resins, nitrocellulose, and epoxy, as well as natural and synthetic rubber.

Epoxy Coatings

Steel will rust and corrode if it is not protected from the elements. One of the most popular steel coatings in the industrial and marine sectors is epoxy. Epoxy coating is used to add an additional layer of protection to steel. A polyamine hardener and an epoxy resin are the two different components that make up an epoxy coating (also known as a catalyst). When combined, the resin and hardener undergo a chemical reaction that causes the components to cross-link as the mixture dries.

Epoxies are known for having excellent adhesion to steel and provide good chemical resistance. They are also often sold as “surface tolerant”, which means they will adhere well to surfaces with minimal surface preparation.

However, the following qualities should be stated and considered when choosing a coating for steel casks (both interior and external):

1. Reliability,
2. Cleanliness,
3. Emission and Absorption,
4. Capability of touch-up and repairs on the loaded (warm) casks.

7.6.2 Literature Survey

7.6.2.1 Introduction

Because of their low cost, high-specific strength/modulus, easy processing, great chemical stability, and light weight, polymers like epoxy-resin are frequently employed as coating materials in the energy sector [71]. Epoxy has good anticorrosion properties, but its λ values, 0.18–0.44 W m^{-1} K^{-1}, are frequently low and cannot meet the demands of highly efficient and quick thermal conduction/dissipation from components like the steel casks used in storage and transportation of SNF [72].

Therefore, the study and development of epoxy and their composites with high-thermal conduction/dissipation capabilities and excellent mechanical properties have urgent theoretical relevance and real-world application values for the development of materials in the energy domains. According to the method of preparation, thermally conductive polymer coatings can be split into two categories: intrinsic type and filled type [67].

Intrinsically Thermally Conductive Epoxy (ITCE) Coatings

In order to increase the intrinsic thermal conductivities of the polymers, ITCE are obtained through special physical structures (such as orientation, liquid crystalline, and crystalline structure) by altering the structures of polymer chain units during the polymer synthesis and processing processes.

Filled-Type Thermally Conductive Epoxy (FTCE) Composites Coatings

FTCE are created by incorporating highly thermally conductive fillers into the polymer matrix and then physically blending the polymers to give them exceptional thermal conductivities.

7.6.2.2 Review of Publications on Anticorrosion Properties and Interfacial Thermal Resistance of Epoxy Composite Coatings

Anticorrosion Property of Epoxy Composites Coatings

Coatings are a frequent, practical, and preferred technique of preventing corrosion in metals [73]. Epoxy composite coatings with fillers have been widely employed as anticorrosion materials, claimed by Zhang et al. [74]. The Metal–Organic Frameworks (MOFs) are useful for a variety of industrial applications due to their unique and varied building units and customizable features [75]. Because of this,

organic polymer coatings based on graphene are used often nowadays as corrosion-prevention techniques.

Graphene and graphene oxide offer a wide range of potential uses in the field of metal protection due to their superior dispersion, chemical activity, and physical barrier capabilities [68], while their barrier features make them suitable for protecting materials [76]. The substantial potential of advanced nanomaterials like graphene oxide as smart containers for the controlled desorption of inhibitors and their performance as dual active/passive anti-corrosive agents in the polymeric composites have been recognized in recent studies by Keshmiri et al. [75]. The effectiveness of graphene and graphene oxide/polymer composite coatings as protective materials is significantly influenced by the interface design in the resin matrix [47].

Despite the extensive research efforts, the existing hydrophobic coating options still have issues, such as weak mechanical strength and limited endurance [54].

The homogenous, 50-m thick epoxy coatings and composite epoxy coatings with 2 wt% of 130-nm silica particles were successfully manufactured in earlier papers on MOF, according to the report by Conradi et al. [77] on austenitic stainless steel of the type AISI 316L. As shown by the increased hardness, increased surface roughness, and induced hydrophobicity, the silica particles were found to significantly improve the microstructure of the coating matrix. In a chloride-ion-rich environment, the silica/epoxy coating was also demonstrated to have excellent anticorrosive performance. This was shown by the fact that the zigzagging of the diffusion path open to the ionic species resulted in a lower rate of corrosion and a higher coating resistance.

Direct mixed oxidation was employed to produce polyaniline (PANI) nanofibers utilizing four various inorganic acids [78]. The findings showed that the Q235 steel is protected to varying degrees by the various composite coatings of PANI doped by various inorganic acids. In conclusion, both the morphology and counter-anion would have an impact on the anticorrosion effect of the doped PANI.

Ghahremani et al. [79] developed a special nano-carrier by modifying the MWCNT surface with polydopamine (PDA), chitosan (CH), and zinc cations. The epoxy coating was improved with the inclusion of the OMWCNT-PDA-CH-Zn nanocomposite, yielding remarkable barrier performance and stable corrosion retardation for nearly 9 weeks.

Motamedi et al.'s [80] innovative nano-pigment, which combines performance epoxy and a nanoceria-decorated cerium (III)-imidazole network (NC/CIN), is similar to a MOF. After 7 weeks of exposure of the intact coating to saline solution, the results showed that the epoxy composite containing NC/CIN offered exceptional barrier-inhibitive protection for mild steel in corrosive environments as well as self-repairing protective properties in the artificially defective nanocomposite (log |Z|10 mHz = 9.91 cm^2).

Titanium dioxide was used to make an epoxy composite (DGPMDAP/MDA/TiO2) in the work by Hsissou et al. [81] in order to examine its rheological and anticorrosion properties. The results showed that adding more TiO_2 improved the rheological properties of DGPMDAP/MDA/TiO2. The epoxy polymer with anticorrosion capabilities decaglycidyl pentamethylene dianiline of phosphorus

(DGPMDAP) displayed mixed-type inhibitor activity and had a maximum corrosive inhibition efficacy of 92% at 103 M (when stationary electrochemical method was used). However, the transient electrochemical method showed that, at 103 M of DGPMDAP, it was a 91% effective carbon steel inhibitor in 1 M HCl solution. The Langmuir isotherm was also used to predict how DGPMDAP adhered to the surface of carbon steel.

In a ground-breaking study by Lashgari et al. [82], ZIF-67 nanoparticles were developed and used as a corrosion inhibitor container to enhance the barrier/active corrosion protection capabilities of the epoxy coating. The protective performance of the ZIF-67 and ZIF-67@APS NPs filled epoxy composites was evaluated utilizing EIS, salt-fog, and cathodic delamination experiments. The coating resistance values of the ZIF-67 and ZIF-67@APS NPs loaded epoxy coatings fell from $3.49 \times 10^{10}\Omega.\ cm^2$ to $2.47 \times 10^{9}\Omega.\ cm^2$ and from $8.16 \times 10^{10}\Omega.\ cm^2$ to $5.78 \times 10^{9}\Omega.\ cm^2$, respectively, after 50 days of immersion. The active corrosion inhibition effect of the epoxy/ZIF-67@APS NPs was demonstrated using electrochemical results.

Chhetri et al. [83] presented an intercalation modification technique to improve the anticorrosion properties of polymeric coatings. The layered double hydroxide (LDH) reservoir was functionalized to increase LDH's interfacial adhesion with the polymer matrix and steel surfaces, and an inhibitor, molybdate, was intercalated to impart inhibitive characteristics. The electrochemical results showed that the addition of functionalized double hydroxide significantly increased the protective efficiency of the epoxy coating. The corrosion protection efficiency of the composite coating was raised by more than 98% and the corrosion rate was decreased by around 98% with the addition of 1 wt% of functionalized LDH.

Cao et al. [84] developed a nano-structured hybrid molecule with strong corrosion inhibitor encapsulating capability and the ability of controlled distribution of benzotriazole in order to simultaneously increase the hydrophobic property and corrosion resistance of epoxy coatings (BTA). Additionally, a film covering the Ce-metal organic frameworks (Ce-MOF), which were developed and used as nanocontainers, was made using tetraethyl orthosilicate (TEOS). The addition of benzotriazole to nanocontainers gave the coating system exceptional anti-corrosion performance. The breakthrough is that the tetraethyl orthosilicate membrane would split and produce pores in an acidic environment, uniformly releasing benzotriazole. This self-healing system used polymer coatings to effectively release a corrosion inhibitor under the control of pH. The results showed that the epoxy coatings with organic frameworks containing 3 wt% Ce-metal had the best anti-corrosion capabilities.

In a 3.5-wt% sodium chloride solution, Wu et al. [85] produced h-BN/SZP aqueous epoxy composite coatings and examined their corrosion protection efficacy. They achieved this by fusing the corrosion-inhibiting ability of strontium zinc phosphate (SZP) with the impermeability of hexagonal boron nitride (h-BN) nanosheets. The anti-corrosion performance of the coatings was evaluated using potential and impedance tests, fitting pore (pinhole) resistance, salt spray, and waterborne epoxy composite coatings applied to mild steels. The analysis of the synthesized (Fh-BN, SZP)/EP coating's localized electrochemical impedance spectroscopy (LEIS) and

corrosion byproducts suggested that the combined effects of h-physical BN's barrier function and SZP's inhibition were responsible for the coated mild steel's superior corrosion resistance. Our method offers a new protection mechanism in coatings for metallic substrates while advancing the fundamental research and industrial uses of h-BN nanosheets.

Interfacial Thermal Resistance of Epoxy Composite Coatings

In thermally conductive polymer composites, interfaces are crucial and significantly affect [86]. The vibration harmonic, acoustic, and modulus mismatch that occurs for phonons at the interfaces during the thermal conduction process leads to severe scattering and a sharp decrease in the phonon's mean free path [87]. According to corresponding macroscopic evidence, the heat flow is frequently partially blocked at the interface, leading to significant heat loss and decreasing the effectiveness of polymer composites [88]. Therefore, in order to further increase the of polymer composites, it will be crucial to enhance the interfaces in thermally conductive polymer composites and minimize interfacial thermal resistance (ITR).

Researchers found that fabricating thermally conductive fillers with heterostructures can significantly reduce the ITR between filler to filler [89, 90].

In order to create hetero-structured Al_2O_3-BNNS thermally conductive fillers, Zou et al. [91] covered the surface of alumina (Al_2O_3) with boron nitride nanosheets (BNNS) before creating thermally conductive Al_2O_3-BNNS/epoxy composites. The value of thermally conductive Al_2O_3-BNNS/epoxy composites reached 2.43 W m^{-1} K^{-1}, higher than pure epoxy-resin (0.21 W m^{-1} K^{-1}), single Al_2O_3/epoxy (1.39 W m^{-1} K^{-1}), and simply blended (Al_2O_3/BNNS)/epoxy (1.94 W m^{-1} K^{-1}) composites under the same fillers amount. This was true when the volume ratio of BNNS to Al_2O_3 was 1:7 and the amount of Al_2O_3/BNNS was 65 vol%.

Further work by Han et al. [92], on the use hetero-structured silicon carbide-BNNS (SiC-BNNS) thermally conductive fillers, proved that fabrication of thermally conductive fillers with hetero-structures corroborated can improve the interfaces between different types of fillers, reduce the phonon scattering at the interfaces and decrease ITR filler to filler.

The thermal characteristics of epoxy-based composites with large loading fractions of electrically conductive graphene fillers and electrically insulating boron nitride fillers randomly orientated were studied by Kargar et al. [93]. It was discovered that at the loading fraction fT > 20 vol%, both types of composites showed a unique thermal percolation threshold. The loading of graphene needed to achieve thermal percolation, fT, was significantly higher than the loading needed to achieve electrical percolation, fE. In terms of improving heat conductivity, graphene fillers fared better than boron nitride fillers. It was determined that heat conduction through the network of percolating fillers dominates thermal transport in composites with large filler loadings, f ≥ fT. Unexpectedly, it was discovered that the

quasi-two-dimensional fillers' cross-plane thermal conductivity had a significant impact on the high-loading composites' thermal transport parameters. The results acquired provide insight into the highly contested mechanism of thermal percolation and aid in the creation of the next generation of effective thermal interface materials for electronic applications.

7.6.2.3 Review of Publications on Neutron Shielding, Anticorrosion Properties and interfacial Thermal Resistance of CuO-NPs-Epoxy Composite Coatings

Neutron Shielding Capacity of Epoxy-CuO-NPs Coatings

The work by Künzel and Okuno [94] examines how particle size, material concentration, and radiation energy affect X-ray absorption. Separately, 5%, 10%, and 30% of the resin mass of a polymeric resin were treated with CuO nanoparticles and microparticles. We investigated the X-ray absorption of these materials using a CdTe detector. The nanostructured material displays more X-ray absorption than the microstructured one for all CuO concentrations.

In the study by Mahmud et al. [95], doping recycled high-density polyethylene (R-HDPE) with phosphotungstic acid (PTA) and CuO-NPs resulted in the creation of an unique (R-HDPE/CuO-NP-PTA) nanocomposite (CuO-NPs). Because the constructed nanocomposites had high-density components including CuO-NPs and phosphotungstic acid, they were discovered to be extremely resistant against rays. When phototungstic acid (PTA) and CuO-NPs were added to R-HDPE, it was discovered that PTA raised the composites' electron density (Nel), mass attenuation coefficient (mm), and effective atomic number (Zeff) more than CuO-NPs did.

According to Abd El-Lateef and Gouda [96], hydrothermal fabrication was successfully used to create new metal oxide–organic frameworks, including cellulose nanocrystals (CNCs), copper oxide/melamine/cellulose nanocrystals (CuO/MEL/CNCs), and nickel oxide/melamine/cellulose nanocrystals (NiO/MEL/CNCs). At 300 mg L^{-1}, the ability to prevent corrosion was determined to be in the following order: NiO/MEL/CNCs (98.3%), CuO/MEL/CNCs (96.8%), and CNCs (85.3%). According to the current study, CNCs and metal oxide-melamine frameworks at CNCs may be viable candidates to prevent AISI360-steel corrosion in the petroleum industry as low-cost, environmentally benign inhibitors.

Hassan and Hashim [97] researched the high-quality and low-cost synthesis of (polystyrene-copper oxide) nanocomposites and studied their structural and optical properties for biological application. The outcomes demonstrated that the nanocomposites have a high-UV region absorption. As the concentration of CuO nanoparticles rises, the attenuation coefficients for the gamma radiation source (Cs-137) do as well.

Thermal Conductivity of Epoxy-CuO-NPs Coatings

Copper oxide nanoparticles (CuO-NPs) with an octahedral morphology that were created using a hydrazine reduction reaction were used to create a new epoxy-based nanocomposite by Sunny et al. [98]. By putting forth a mechanism based on the distribution of nCOP domains in the epoxy matrix and the current volume of restricted epoxy chains, the behavior of epoxy-nCOP nanocomposites has been explained in this study.

A novel epoxy-based nanocomposite material was created using nanosized copper (I) oxide particles (nCOP) created through a chemical reduction reaction, according to Sunny et al. [99]. The shape and microstructure development in the nanocomposites have been associated with the tuning of the epoxy resin's hydrophilicity in the presence of variable nCOP content.

Rajendren and Subramani [100] claim that making epoxy materials into good conducting materials for extremely complex applications can make them more appealing. Cu/CNT composite powder increases the thermal stability of epoxy composites while lowering onset temperature as CNT concentration in Cu is increased. Epoxy composites with the highest thermal conductivity and shore hardness were found to have values of 0.253 W/mK and 83.3 ± 0.4, respectively, with corresponding improvements of 24.3 and 10% over pure epoxy. Regardless of the Cu-CNT concentration, the maximum value of epoxy-based composites is attained at 1.0 Epoxy/Comp25 composites and is then reduced.

According to Jasim et al. [101], polymeric composites are among the most isolated materials, yet they also offer a high degree of mechanical flexibility. The findings indicate that at 65% EP + 35% Cu the highest glass transition temperature (T_g) of (EP/Cu) composites was 58.949 °C. Hardness increases as copper concentration rises, reaching a maximum of 83.9 for (55%EP + 45%Cu). To match the warm summer temperatures in our country, this composite can be used to coat surfaces and floors.

Anticorrosion and Mechanical Properties of Epoxy-CuO-NPs Coatings

According to Nazari et al. [102], a number of techniques have been used to shield metal assets against corrosion damage, one of which is the use of very effective and affordable organic coatings. It has been found that the most promising nanofillers for enhancing the barrier performance of organic coatings are those that are carbon- and bio-based. As they could be controlled to release mending or protective compounds, primarily to corrosion faults or damaged parts of the coating once triggered by external stimuli, smart nanocomposite organic coatings were then investigated. Then, superior and long-lasting corrosion protection offered by high-performance nanocomposite organic coatings was looked at. Then, sophisticated characterization techniques for researching organic nanocomposite coatings were briefly covered. We wrapped up by summarizing the major discoveries and the unmet research requirements.

Zhang et al. [103], by using electrochemical impedance spectroscopy (EIS), Fourier transform infrared spectroscopy (FTIR), and scanning electron microscope (SEM/EDS) methods, the degradation processes of two self-polishing antifouling coatings containing copper-based agents (CuSCN and Cu_2O) in 3.5% NaCl solution as well as the protection effect of the coating systems were investigated. The findings show that the two coating systems still have extremely good protective properties for the 5083 Al alloy substrate after immersion for 1525 days at room temperature, as seen by the high value of the low-frequency impedance. The antifouling topcoat suffers severe damage from the alternate high- and low-temperature immersion test (45 °C for 12 h + 25 °C for 12 h), and the failure is primarily characterized by numerous micro-pores and micro-cracks. The micro-pores created after the agents were dissolved and released during the hydrolysis process of the antifouling coating are relatively larger, because the CuSCN antifouling agent particle has a larger diameter and a slightly higher solubility than the Cu_2O agent. This causes a greater decrease in impedance and a worse protective property of the coating system for the substrate.

In order to demonstrate the benefits of incorporating CuO nanofillers into the epoxy resin polymer, a comparison study (structural, thermal, mechanical, and electrical) between the neat-epoxy resin polymer matrix and the epoxy resin polymer decorated with (Ag-CuO) nanoparticles (NPs) and (Mg-CuO) nanosheets has been conducted by El-Masry and Imam [104]. It was shown that the interaction of (Ag-CuO) nanoparticles or (Mg-CuO) nanosheets with epoxy networks enhanced the physical/chemical properties of neat-epoxy by providing it a new, captivating performance that satisfies the requirements of advanced applications. Epoxy plastic's behavior was altered by Mg-CuO nanofillers to exhibit the ductile feature. Epoxy's thermal stability, electrical conductivity, dielectric constant, and lowest activation energy were all increased by (Ag-CuO) NPs. A low-cost option for usage in numerous electrical applications is the Ag-CuO/Epoxy nanocomposite. On the stress–strain curve, Mg-CuO/Epoxy has a broader elasticity region. In comparison to the individual constituent phases and the matrix, the hybrid nanocomposite between neat-epoxy and (Ag/Mg-CuO) NPs presents the solution for more functional applications.

7.6.2.4 Thermal Conduction Models and Inner Mechanisms of Thermally Conductive Epoxy Composite

The following are some of the most successful thermal conduction models that have been proposed by researchers.

For filled polymers with particles, Agari and Uno [105] suggested a new thermal conduction model, and projected values from the new model are compared with experimental results. The model is basically based on a generalization of composite parallel and series conduction models, which has been further refined to account for the isotropy of heat conduction in a random dispersion system. The new model yields the following equation: $\log\lambda = V \cdot C_2 \cdot \log\lambda_2 + (1 - V) \cdot \log(C_1 \cdot \lambda_1)$. As a result,

the equation may be used to estimate the thermal conductivity of the filled polymer (λ) with any volume content (V) of particles when the thermal conductivities of the polymer and particles (λ_1, λ_2) are known. Experimental results for polyethylene, polystyrene, and polyamide are filled with graphite, copper, or Al_2O_3.

This study by Agrawal and Satapathy [106] investigates ways to improve the ability of aluminum nitride-loaded epoxy composites to conduct heat. In order to build a theoretical model for one-dimensional heat conduction through such a composite, the laws of least thermal resistance and specific equivalent thermal conductivity were combined. The values obtained using the suggested mathematical correlation were compared with experimental findings that were measured as well as with values that were estimated using other well-known correlations such the Rule-of-Mixture, Maxwell's model, Bruggeman model, and Nielson-Lewis model. This comparison shows that although none of the aforementioned models are capable of accurately forecasting the composites' effective thermal conductivity, the outcomes of the proposed model that incorporates a correction factor are in decent accordance with the experimental results.

Conclusion on Literature Review

There are always some discrepancies between the predicted values by models and the experimental values because the current thermal conduction models only have a limited application range and do not account for ITR, shape, amount, and surface properties of thermally conductive fillers, among other factors. Future research on thermal conduction models must fully take into account additional practical influencing factors, quantify them, and incorporate them into the models in order to increase the degree of agreement between the models and the experimental data.

This will result in the establishment of general mathematical models on interfacial thermal resistance for novel shapes and properties of thermally conductive epoxy composites.

7.7 Methodology

7.7.1 Materials and Methods

7.7.1.1 Materials

WCD

The WCD from SA will serve as the raw material for the creation of CuO-NPs with various compositions.

Epoxy-Resin

The two major elements of the ultraviolet curable coatings will be epoxy acrylate and tripropylene glycol diacrylate, while vinyltrimethoxysilane and castor oil will function as plasticizers and coupling agents, respectively.

Steel

The substrate for this study will be mild steel sheets (7 × 3.5 × 0.1 cm).

7.7.1.2 Methods

The WCD will first go through gravity separation to create concentrates with varied copper oxide, aluminum oxide, and silicon oxide contents as explained in the following sub-sections.

Density Separation of WCD

To separate the WCD based on densities, the rotational bowl speed and fluidized water flow rate will be altered at three levels (Table 7.1). Table 7.2 details the test process for the density separation of the WCD. After five passes through the separator, 45 test samples will be generated (Table 7.3). These concentrates will be used as the basic ingredient in the production of copper precursors. The calculations that will be performed before creating the slurry that will be used for the density separation experimentation are described in detail in Okanigbe's thesis [107].

Design of Experiment and Procedure for Production of Copper Precursor from Concentrates

Manufacturing of CuO-NPs started with the production of copper precursor from leached concentrates. The experiment design for the production of copper precursor from leached concentrates was developed using the 3 × 2 complete factorial experimental design approach, as shown in Tables 7.4 and 7.5.

The copper precursor will be created by adding dropwise 2 M Na_2CO_3 solution to 0.2 M $CuSO_4$ solution in a 500-ml conical flask positioned on a hot plate while

Table 7.1 Parameters measured for density separation experiment

S.N	Parameters	Low (0)	Medium (1)	High (2)
X_1	RBS (m/s^2)	60	90	120
X_2	FWFR (l/min)	3.0	4.5	6.0

Table 7.2 Test protocol for density separation of CSD

Tests	RBS (G)	FWFR (l/min)	Treatment combination (TC)
1	A	A	AA
2	A	B	AB
3	A	C	AC
4	B	A	BA
5	B	B	BB
6	B	C	BC
7	C	A	CA
8	C	B	CB
9	C	C	CC

Table 7.3 Test protocol for production of concentrates with different copper oxide, aluminum oxide, and silicon oxide contents

	Tests and tailings								
Passes	(1)	(2)	(3)	(4)	(5)	(6)	(7)	(8)	(9)
1	1(1)	1(2)	1(3)	1(4)	1(5)	1(6)	1(7)	1(8)	1(9)
2	2(1)	2(2)	2(3)	2(4)	2(5)	2(6)	2(7)	2(8)	2(9)
3	3(1)	3(2)	3(3)	3(4)	3(5)	3(6)	3(7)	3(8)	3(9)
4	4(1)	4(2)	4(3)	4(4)	4(5)	4(6)	4(7)	4(8)	4(9)
5	5(1)	5(2)	5(3)	5(4)	5(5)	5(6)	5(7)	5(8)	5(9)

stirring the mixture with a magnetic stirrer at various temperatures (Fig. 7.4). The resulting green precipitate will be separated by filtration and then washed with distilled water and pure ethanol. The green precipitate will then be dried in a 105 °C oven for 24 h.

Design of Experiment and Procedure for Production of CuO-NPs from Copper Precursor

On the basis of an air flow and a thermogravimetric analyzer, the thermal behavior of the synthesized copper precursor will be measured. A platinum crucible containing 35 mg of samples will be placed on the microbalance pan and heated at rates of 5, 10, 15, and 20 °C/min between 25 and 1000 °C.

The investigation will be conducted using a 3 × 2 complete factorial experimental design method (Tables 7.4 and 7.5). After familiarizing oneself with the thermal behavior of the copper precursor, Tables 7.6 and 7.7 show how the experiment will be planned based on the data for the generation of CuO-NPs. An experimental approach can be found in Okanigbe [107].

Table 7.4 Parameters considered for the production of copper precursor

Parameters	Levels		
	Low	Medium	High
Temperature (°C)	25	55	85
Rotational speed (rpm)	340	740	1480

Table 7.5 The design of experiment for the production of copper precursor

Tests	Temperature (°C)	Rotational speed (rpm)	Treatment combinations (TC) (°C/rpm)
1	25	340	25/340
2	25	740	25/740
3	25	1480	25/1480
4	55	340	55/340
5	55	740	55/740
6	55	1480	55/1480
7	85	340	85/340
8	85	740	85/740
9	85	1480	85/1480

Preparation and Polymerization of Hybrid Nanocomposite Coatings by Electron Beam Radiation

Six solvent-free coating formulations (blank L_0) will be created using epoxy acrylate (EA) oligomer as the binder, TPGDA as the thinner, CO as the plasticizer, and VTMS as the coupling agent. Developed coating formulations (hybrid) will be measured against blank L_0 to determine performance enhancement. Different CuO-NP compositions (CuO, and other trace oxides wt%) will be added to the formulations L-1(1) to L-5(9) as shown in Table 7.8. These different compositions will be used to create hybrid organic–inorganic composite coatings. These hybrid formulations will then be homogenized using a homogenizer at room temperature after being sonicated for 20 min and lightly blended for a further 15 min at 10.000 revolutions per minute (rpm). Using a film applicator (Elcometer 3540, USA), all hybrid formulations will then be applied as thin films with a thickness of 100 mm onto steel panels and subsequently polymerized with a dose of 10 kGy of electron beam irradiation.

Development of Predictive Models

Modeling Technique for Predictive Output

The fundamental processes used in the modelling approach described in this research are presented in this subsection:

Step 1: Analyze the trends in the experimental samples.

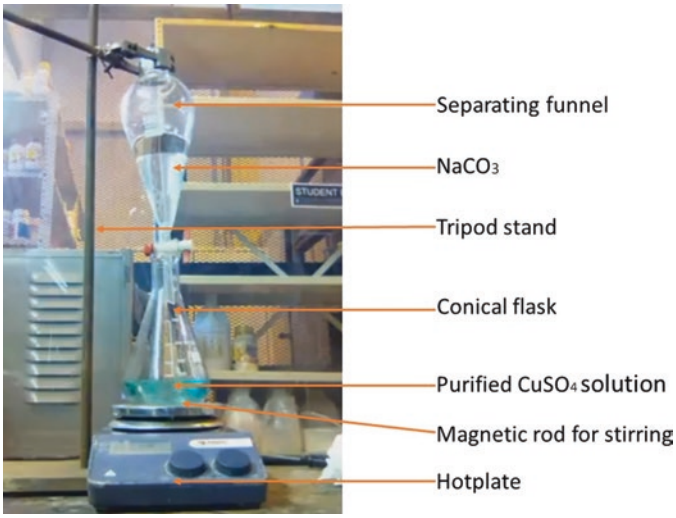

Fig. 7.4 Experimental set-up for the production of copper precursor

Table 7.6 Parameters considered for the production of CuO-NPs

	Levels		
Parameters	Low	Medium	High
Temperature (°C)	650	750	850
Time (h)	1	2	3

Step 2: Establish constraint models to classify and divide samples into sub-classes in accordance with Step 1.
Step 3: Calculate the absolute difference between input and output samples belonging to the same class as those classified in Step 2.
Step 4: Determine various experimental levels for the classes.
Step 5: Predict output using an interpolant model.
Step 6: Finish.

Table 7.9 contains a generalized form of the modeling variables. The possible effects of the various mineral constituents observed in the experimental concentrations were calculated using a model that took these variables into account. The modeling strategy discussed here is based on the constrained interpolation of findings from any three sequential experimental samples. Two of these outputs are frequently known by experience, and predictive modeling is used to identify the third unknown output. First and second columns of Table 7.9 display the ordered experimental trials that are used for interpolation. The (%) proportions of the inputs (p_{i_1} , p_{i_2} , and p_{i_3}) and outputs (p_{o_1} , p_{o_2} , and p_{o_3}) for the investigated mineral constituents are shown in the third and fourth columns, respectively. Additionally, for each of the three experimental samples under examination, column six shows the

Table 7.7 The design of experiment for production of copper nanoparticles

Tests	Temperature (°C)	Time (h)	TC (°C/h)
1	650	1	650/1
2	650	2	650/2
3	650	3	650/3
4	750	1	750/1
5	750	2	750/2
6	750	3	750/3
7	850	1	850/1
8	850	2	850/2
9	850	3	850/3

absolute difference between the input and output values stated in terms of, and column five shows the experimental levels.

The following under listed are modelling notations as presented in this research:

$$\text{Output} = f\left(\text{speed}, \text{flow rate}, \text{input}, \text{feed rate}, \text{liquid solid ratio}\right)$$

Let: serial number for inputs: $s_{\text{i}} = \{1, \ldots, n-1, n\}$ and serial number for outputs$s_{\text{o}} = \{1, \ldots, n-1, n\}$ for $\forall n \in R$.

Where:

$\exp_{(\text{i})i,\,j}$ = Experimental inputs,
$\exp_{(\text{o})i,\,j}$ = Experimental outputs,
$\text{Pre}_{(\text{o})i,\,j}$ = Predictive outputs,
p_{i_j} = % input proportion of selected samples,
p_{o_j} = % output proportion of selected samples,
$\Delta p_j = \left| p_{\text{i}_j} - p_{\text{o}_j} \right|$ absolute difference between p_{i_j} and p_{o_j}

Where $j = \{1, \ldots, k-1, k\}$ represents experimental levels.

The "absolute difference" models defined in terms of the experimental levels are shown in Eqs. (7.1) through (7.3), and the final computational models for projecting the unknown outputs are shown in Eqs. (7.4) through (7.6) with respect to Table 7.9.

$$\Phi_1 = \left[\frac{\Phi_3\left(\mu - \xi\right) - \Phi_2\left(\mu - \xi\right) - \Phi_2\left(\sigma - \mu\right)}{\left(\mu - \sigma\right)} \right] \tag{7.1}$$

$$\Phi_2 = \left[\frac{\Phi_3\left(\mu - \xi\right) + \Phi_1\left(\sigma - \mu\right)}{\left(\sigma - \mu\right) + \left(\mu - \xi\right)} \right] \tag{7.2}$$

$$\Phi_3 = \left[\frac{\Phi_1\left(\mu - \sigma\right) + \Phi_2\left(\sigma - \mu\right) + \Phi_2\left(\mu - \xi\right)}{\left(\mu - \xi\right)} \right] \tag{7.3}$$

Table 7.8 Compositional formulations of different epoxy-CuO-NPs coatings

	Compositional formulations						
Coating	EA (wt%)	TPGDA (wt%)	CO (wt%)	Total	VTMS (wt%)	CuO-NPs (wt%)	Irradiation dose (kGy)
Blank (L_0)	70	20	10	100	1	0.5	10
L-1(1)	70	20	10	100	1	0.5	10
L-1(2)	70	20	10	100	1	0.5	10
L-1(3)	70	20	10	100	1	0.5	10
L-1(4)	70	20	10	100	1	0.5	10
L-1(5)	70	20	10	100	1	0.5	10
L-1(6)	70	20	10	100	1	0.5	10
L-1(7)	70	20	10	100	1	0.5	10
L-1(8)	70	20	10	100	1	0.5	10
L-1(9)	70	20	10	100	1	0.5	10
L-2(1)	70	20	10	100	1	0.5	10
L-2(2)	70	20	10	100	1	0.5	10
L-2(3)	70	20	10	100	1	0.5	10
L-2(4)	70	20	10	100	1	0.5	10
L-2(5)	70	20	10	100	1	0.5	10
L-2(6)	70	20	10	100	1	0.5	10
L-2(7)	70	20	10	100	1	0.5	10
L-2(8)	70	20	10	100	1	0.5	10
L-2(9)	70	20	10	100	1	0.5	10
L-3(1)	70	20	10	100	1	0.5	10
L-3(2)	70	20	10	100	1	0.5	10
L-3(3)	70	20	10	100	1	0.5	10
L-3(4)	70	20	10	100	1	0.5	10
L-3(5)	70	20	10	100	1	0.5	10
L-3(6)	70	20	10	100	1	0.5	10
L-3(7)	70	20	10	100	1	0.5	10
L-3(8)	70	20	10	100	1	0.5	10
L-3(9)	70	20	10	100	1	0.5	10
L-4(1)	70	20	10	100	1	0.5	10
L-4(2)	70	20	10	100	1	0.5	10
L-4(3)	70	20	10	100	1	0.5	10
L-4(4)	70	20	10	100	1	0.5	10
L-4(5)	70	20	10	100	1	0.5	10
L-4(6)	70	20	10	100	1	0.5	10
L-4(7)	70	20	10	100	1	0.5	10
L-4(8)	70	20	10	100	1	0.5	10
L-4(9)	70	20	10	100	1	0.5	10
L-5(1)	70	20	10	100	1	0.5	10
L-5(2)	70	20	10	100	1	0.5	10

(continued)

Table 7.8 (continued)

Coating	Compositional formulations						
	EA (wt%)	TPGDA (wt%)	CO (wt%)	Total	VTMS (wt%)	CuO-NPs (wt%)	Irradiation dose (kGy)
L-5(3)	70	20	10	100	1	0.5	10
L-5(4)	70	20	10	100	1	0.5	10
L-5(5)	70	20	10	100	1	0.5	10
L-5(6)	70	20	10	100	1	0.5	10
L-5(7)	70	20	10	100	1	0.5	10
L-5(8)	70	20	10	100	1	0.5	10
L-5(9)	70	20	10	100	1	0.5	10

Table 7.9 Generalized representation of model variables

Level	Data acquisition procedure	Input value for variant factor p_{i_j}	Output value for variant factor p_{o_j}	Expt. levels	Absolute difference between p_{i_j} and p_{o_j}
1-First	Prediction	p_{i_1}	p_{o_1}	ξ	$\lvert p_{i_1} - p_{o_1} \rvert = \Phi_1$
2-Second	Experiment	p_{i_2}	p_{o_2}	μ	$\lvert p_{i_2} - p_{o_2} \rvert = \Phi_2$
3-Third	Experiment	p_{i_3}	p_{o_3}	σ	$\lvert p_{i_3} - p_{o_3} \rvert = \Phi_3$

$$\left| p_{i_1} - p_{o_1} \right| = \Phi_1 \tag{7.4}$$

$$\left| p_{i_2} - p_{o_2} \right| = \Phi_2 \tag{7.5}$$

$$\left| p_{i_3} - p_{o_3} \right| = \Phi_3 \tag{7.6}$$

Hence, $\Delta p_j = \Phi_j$.

Experimental Validation and Simulation

The epoxy-CuO-NPs composite coatings thermal conductivity, anticorrosion, and mechanical properties will be experimentally determined in order to validate the expected ideal composition of the organic–inorganic composite coating.

Characterization of the Developed Epoxy-CuO-NPs Composite Coatings

All coated films will be characterized using the following:

1. Fourier transform infrared spectroscopy,
2. Transmission electron microscopy,

3. Thermogravimetric analyzer,
4. X-ray diffraction,
5. Scanning electron microscopy,
6. UV–Vis–NIR spectroscopy,
7. Atomic force microscope,
8. Contact angle meter.

Measurement of the Basic Properties of the Developed Epoxy-CuO-NPs Composite Coatings

For each of the following listed measurements, the average of five readings will be calculated:

1. Hardness measurement
2. Bending measurement
3. Adhesion measurement
4. Glossiness measurement
5. Coating steel scratch measurement
6. Acid/alkali resistance measurement

Corrosion Tests

According to ASTM, corrosion tests for hybrid coating films were estimated as follows: the degree of rust under the coated film was determined according to ASTM D 610–01; the degree of blistering under the coated film was performed according to ASTM D 714–7 (2000), and the degree of adhesion failure of the X-cut was made according to ASTM D 1654–92 (2000).

Weight Loss Measurements

Mild steel sheets measuring 3 × 3 × 0.1 cm were used. The steel sheets have been thoroughly cleaned and weighed. The following Eq. (7.7) will be used to get the average weight reduction for coated steel:

$$W = \left(W_1 - W_2\right) / S, \tag{7.7}$$

where W is the average weight loss (mg/cm^2), W_1 is the average weight loss of the coated steel before immersion, W_2 is the average weight loss of the coated steel after immersion, and S is the total area of the mild steel panel.

The plates in the current investigation will be removed from sodium chloride (NaCl) solution at the intervals of 10, 20, 30, and 60 days in accordance with ASTM D 2688-94 (1999). Analyses of the electrochemical kind Galvanic charge/discharge measurements will be carried out using a Biologic SP300 and three electrodes. After 30 days of exposure to a 3.5% NaCl solution, the hybrid-coated steel plates will be removed, and the open circuit potential will be measured over the frequency range of 0.1–103 Hz with an amplitude of 10 mV.

Thermal Conductivity Measurements

Using a test rig apparatus, the epoxy coating's thermal conductivity will be determined at various concentrations of copper nanoparticles. A thermocouple, a uniform plate heater with a resistance, a voltage control, a switch, and a temperature reader will be included in this test apparatus.

7.8 Contribution to Knowledge

At the end of the investigation, the following details will be made public:

1. The creation of a brand-new epoxy/CuO-NPs composite coating.
2. For improved heat conductivity and anticorrosion of mild steel, hence this composite coating has not yet been used in the design of cask for transportation of SNF.
3. As a result, the composition is brand-new.
4. The availability of WCD, a fresh secondary supply of CuO-NPs, enabling the creation of organic–inorganic coatings.
5. WCD is a secondary resource that has not been utilized as an inorganic material to improve the thermal conductivity and anticorrosion of mild steel.
6. The CuO-NPs substance is therefore brand-new.

7.9 Ethical Considerations

This project has no unethical components.

7.10 Dissemination

The Department of Higher Education and Training (DHET) recognized journals listed below are just a few that will publish the findings of the study:

1. Nano-micro Letter, Publisher: Springer
2. Journal of Metals, Publisher: Springer

Additionally, the findings will be presented at national and international conferences in addition to being published in full in the conference proceedings.

7.11 Budget and Time Frame

7.11.1 Budget

The estimated budget for this proposed study can be seen in Table 7.10.

7.11.2 Time Frame

The estimated time for the completion of this proposed study can be seen in Table 7.11.

Table 7.10 Estimated budget of the project

Items	Cost (R)	Source
Literature sourcing and stationaries	To be estimated	X
Materials and supplies	To be estimated	X
Analytical equipment	To be estimated	X
Travelling expenses	To be estimated	X
Miscellaneous expenses	To be estimated	X
Total		X

Key: TUT = Tshwane University of Technology; R = Rand

Table 7.11 Estimated time frame of the project

S.N	Task name	Year	
1	Proposal (compilation and presentation)	WIP	WIP
2	Literature review	WIP	WIP
3	Material sourcing	WIP	WIP
4	Sample preparation (sampling)	WIP	WIP
5	Fabrication of test samples optimization process	WIP	WIP
6	Fabrication of test samples	WIP	WIP
7	Thermal conductivity and wear resistance tests	WIP	WIP
8	Results, data, and analysis	WIP	WIP
9	Optimum predictive model development	WIP	WIP
10	3D print of brake rotor and validation of optimum prediction	WIP	WIP
11	Compilation and presentation of final report	WIP	WIP

Key: WIP = Work in progress

References

1. M.K. Nematchoua, J.A. Orosa, Life cycle assessment of radioactive materials from a residential neighbourhood. Sustain. Mater. Technol. **33**, e00468 (2022)
2. G. Vaidyanathan, R.D. Kale, India's nuclear power program: A critical review. Sādhanā **47**(3), 1–18 (2022)
3. T.A. Kurniawan, M.H.D. Othman, D. Singh, R. Avtar, G.H. Hwang, T. Setiadi, W.H. Lo, Technological solutions for long-term storage of partially used nuclear waste: A critical review. Ann. Nucl. Energy **166**, 108736 (2022)
4. T. Sakuragi, T. Okamura, R. Hamada, H. Asano, E. Minari, M. Nakase, K. Takeshita, T. Oniki, M. Uchiyama, Optimal waste loading in high-level nuclear waste glass from high-burnup spent fuel for waste volume and geological disposal footprint reduction. MRS Adv. **7**(7), 150–154 (2022)
5. M.S. Yim, Characteristics of spent fuel and its storage and transportation, in *Nuclear Waste Management*, (Springer, Dordrecht, 2022), pp. 257–339
6. M.S. Yim, Spent fuel reprocessing and nuclear waste transmutation, in *Nuclear Waste Management*, (Springer, Dordrecht, 2022), pp. 341–384
7. M.S. Yim, Management of low and intermediate level waste, in *Nuclear Waste Management*, (Springer, Dordrecht, 2022), pp. 635–685
8. M. Alwaeli, V. Mannheim, Investigation into the current state of nuclear energy and nuclear waste management—A state-of-the-art review. Energies **15**(12), 4275 (2022)
9. A. Yadav, A. Singh, A. Shukla, Nuclear energy and conventional clean fuel, in *Status and Future Challenges for Non-conventional Energy Sources*, vol. 1, (Springer, Singapore, 2022), pp. 23–44
10. Safety Series No. 6, *Regulations for the Safe Transport of Radioactive Materials* (International Atomic Energy Agency, Vienna, 1985)
11. Standard Safety Series No. TS-R-1, *Regulations for the Safe Transport of Radioactive Materials* (International Atomic Energy Agency, Vienna, 2003)
12. Standard Safety Series, *Transportation of Spent Research Reactor Fuel to USA* (Phoenix, 2011)
13. S. Kang, D.H. Kim, Y.S. Chang, S. Lee, Integrity assessment of spent fuel assembly in vertically and obliquely dropping cask. J. Mech. Sci. Technol. **35**(9), 3821–3827 (2021)
14. D. Grgić, M. Matijević, P. Dučkić, R. Ječmenica, Analysis of the HI-TRAC VW transfer cask dose rates for spent fuel assemblies loaded in nuclear power plant Krsko storage campaign one. J. Nucl. Eng. Radiat. Sci. **8**(4), 041902 (2022)
15. Y. Liu, B. Craig, Z. Han, J. Li, K. Byrne, H. Takeda, T. Saegusa, RAMM-TM for detection of gas leakage from canisters containing spent nuclear fuel. Nucl. Eng. Des. **385**, 111534 (2021)
16. A. Knight, B. Nation, C. Bryan, R. Schaller, *FY21 Status Report: SNF Canister Coatings for Corrosion Prevention and Mitigation*. (No. SAND2021-10810R) (Sandia National Lab (SNL-NM), Albuquerque, 2021)
17. P. Goyal, V. Verma, A. Dutta, J. Chattopadhyay, Quantification of lead melting in a radioactive transport cask using CFD. *BARC Newsletter* (2021)
18. L. Vergari, M. Fratoni, Spent fuel management strategies for fluoride-cooled pebble bed reactors. Nucl. Eng. Des. **378**, 111189 (2021)
19. M.G. El-Samrah, A.F. Tawfic, S.E. Chidiac, Spent nuclear fuel interim dry storage; design requirements, most common methods, and evolution: A review. Ann. Nucl. Energy **160**, 108408 (2021)
20. I.M. Mousaa, N.A. Abdelreheim, S.A. Elnaggar, R.M. Fathy, Green synthesis and use of copper oxide nanoparticles to prepare a highly thermal, antimicrobial, and anticorrosion hybrid coating for mild steel under electron beam irradiation. Anti-Corros. Methods Mater. **69**(2), 160–170 (2022)
21. G.Y. Shkoukani Al-Qous, *Shielding and Corrosion Behavior of Materials in Nuclear Applications* (North Carolina State University ProQuest Dissertations Publishing, 2021)

22. D. Asefi, M. Arami, N.M. Mahmoodi, Electrochemical effect of cationic gemini surfactant and halide salts on corrosion inhibition of low carbon steel in acid medium. Corros. Sci. **52**(3), 794–800 (2010)
23. I.M. Mousaa, N.M. Ali, M.K. Attia, Preparation of high performance coating films based on urethane acrylate oligomer and liquid silicone rubber for corrosion protection of mild steel using electron beam radiation. Prog. Org. Coat. **155**, 106222 (2021)
24. T. Wang, Q. Guo, T.C. Zhang, Y.X. Zhang, S. Yuan, Large-scale prepared superhydrophobic HDTMS-modified diatomite/epoxy resin composite coatings for high-performance corrosion protection of magnesium alloys. Prog. Org. Coat. **170**, 106999 (2022)
25. O. Mazzantini, F. D'Auria, J.R. Riznic, Atucha II plant description, in *Pressurized Heavy Water Reactors*, (Elsevier, 2022), pp. 1–49
26. K.A. Ross, M. Pole, B. Gwalani, T.J. Montoya, R. Schaller, E. Karasz, *Cold Spray for Mitigation and Repair of Spent Nuclear Fuel Dry Storage Canisters*. (No. PNNL-32917) (Pacific Northwest National Lab (PNNL), Richland, 2022)
27. S.G. Acharyya, A. Khandelwal, V. Kain, A. Kumar, I. Samajdar, Surface working of 304L stainless steel: Impact on microstructure, electrochemical behavior and SCC resistance. Mater. Charact. **72**, 68–76 (2012)
28. ASTM Standard, *Standard Test Methods for Determining Area Percentage Porosity in Thermal Sprayed Coatings* (ASTM International, West Conshohocken, 2014), pp. 2–8
29. J. Fiebig, E. Bakan, T. Kalfhaus, G. Mauer, O. Guillon, R. Vaßen, Thermal spray processes for the repair of gas turbine components. Adv. Eng. Mater. **22**(6), 1901237 (2020)
30. S. Ghosh, V. Kain, Effect of surface machining and cold working on the ambient temperature chloride stress corrosion cracking susceptibility of AISI 304L stainless steel. Mater. Sci. Eng. A **527**(3), 679–683 (2010)
31. S.W. Glass, M.R. Larche, M.S. Prowant, J.D. Suter, J.P. Lareau, X. Jiang, K.A. Ross, Cold spray NDE for porosity and other process anomalies, in *AIP Conference Proceedings*, vol. 1949, no. 1, (AIP Publishing LLC, 2018), p. 020010
32. M.R. Rokni, C.A. Widener, O.C. Ozdemir, G.A. Crawford, Microstructure and mechanical properties of cold sprayed 6061 Al in As-sprayed and heat treated condition. Surf. Coat. Technol. **309**, 641–650 (2017)
33. B. Hanson, H. Alsaed, C. Stockman, D. Enos, R. Meyer, K. Sorenson, *Gap Analysis to Support Extended Storage of Used Nuclear Fuel*. (No. PNNL-20509) (2012)
34. R. Hosler, J. Hall, *Outside Diameter Initiated Stress Corrosion Cracking*. (No. PA-MSC-0474) (2010)
35. J.P. Lareau, *Operating Experience with Chloride Induced Stress Corrosion Cracking*. (EPRI ESCP) (2014)
36. A.W. Knight, R. Schaller, C.R. Bryan, T.J. Montoya, A.M. Parey, J. Carpenter, M. Maguire, K. Ross, *Corrosion-Resistant Coatings for Mitigation and Repair of Spent Nuclear Fuel Dry Storage Canisters*. (No. SAND-2020-7916R) (Sandia National Lab (SNL-NM), Albuquerque, 2020)
37. S.J. Saltzstein, B. Hanson, G.A. Freeze, *Spent Fuel and Waste Science and Technology Storage and Transportation R&D Strategic Plan*. (No. SAND2020-11667C) (Sandia National Lab (SNL-NM), Albuquerque, 2020)
38. C.R. Bryan, D.G. Enos, *Analysis of Dust Samples Collected from Spent Nuclear Fuel Interim Storage Containers at Hope Creek, Delaware, and Diablo Canyon, California*. (No. SAND2014-16383) (Sandia National Lab (SNL-NM), Albuquerque, 2014)
39. C.R. Bryan, D. Enos, *Analysis of Dust Samples Collected from an Unused Spent Nuclear Fuel Interim Storage Container at Hope Creek, Delaware*. (No. SAND-2015-1746) (Sandia National Lab (SNL-NM), Albuquerque, 2015)
40. C.R. Bryan, A.W. Knight, *Analysis of Dust Samples Collected from an Inland ISFSI Site (Site A)*. (No. SAND-2020-13674) (Sandia National Lab (SNL-NM), Albuquerque, 2020)

41. C.R. Bryan, E.J. Schindelholz, *Analysis of Samples Collected from the Surface of Interim Storage Canisters at Calvert Cliffs in June 2017: Revision 01*. (No. SAND2017-12429) (Sandia National Lab (SNL-NM), Albuquerque, 2017)
42. C.R. Bryan, E.J. Schindelholz, *FY18 Status Report: SNL Research into Stress Corrosion Cracking of SNF Interim Storage Canisters*. (No. SAND-2018-12595R) (Sandia National Lab (SNL-NM), Albuquerque, 2018)
43. R.F. Schaller, A.W. Knight, C. Bryan, B. Nation, T.J. Montoya, R.M. Katona, *FY20 Status Report: SNF Interim Storage Canister Corrosion and Surface Environment Investigations*. (No. M2SF-21SN010207055) (US Department of Energy. Sandia National Laboratories, Albuquerque, 2020)
44. E.J. Schindelholz, C.R. Bryan, C.L. Alexander, *FY17 Status Report: Research on Stress Corrosion Cracking of SNF Interim Storage Canisters*. (No. SAND-2017-10338R) (Sandia National Lab (SNL-NM), Albuquerque, 2017)
45. A. Knight, C. Bryan, *Analysis of Dust Samples Collected from an Inland ISFSI Site ("Site B")*. (No. SAND2020-14144) (Sandia National Lab (SNL-NM), Albuquerque, 2020)
46. C.R. Bryan, D.G. Enos, *Interim Storage Environment: Considerations for Corrosion Testing of SNF Dry Storage Containers*. (No. SAND2013-3519C) (Sandia National Lab (SNL-NM), Albuquerque, 2013)
47. H. Wu, L. Cheng, C. Liu, X. Lan, H. Zhao, Engineering the interface in graphene oxide/epoxy composites using bio-based epoxy-graphene oxide nanomaterial to achieve superior anticorrosion performance. J. Colloid Interface Sci. **587**, 755–766 (2021)
48. Y. Hu, L. Zeng, A.J. Minnich, M.S. Dresselhaus, G. Chen, Spectral mapping of thermal conductivity through nanoscale ballistic transport. Nat. Nanotechnol. **10**(8), 701–706 (2015)
49. Y. Lin, Y. Jia, G. Alva, G. Fang, Review on thermal conductivity enhancement, thermal properties and applications of phase change materials in thermal energy storage. Renew. Sust. Energ. Rev. **82**, 2730–2742 (2018)
50. M.K. Hassanzadeh-Aghdam, R. Ansari, H.M. Deylami, Influence of graphene nano-platelets on thermal transport performance of carbon fiber-polymer hybrid composites: Overall assessment of microstructural aspects. Int. J. Therm. Sci. **171**, 107209 (2022)
51. M.K. Hassanzadeh-Aghdam, R. Ansari, A micromechanics-based hierarchical analysis of thermal conductivity of metallic nanocomposites with agglomerated ceramic nanoparticles. Arab. J. Sci. Eng. **46**(8), 7143–7151 (2021)
52. J. Park, D. Kim, H. Kim, J. Lee, W. Chung, Thermal radiative copper oxide layer for enhancing heat dissipation of metal surface. Nanomaterials **11**(11), 2819 (2021)
53. M. Ramezanzadeh, B. Ramezanzadeh, Thermomechanical and anticorrosion characteristics of metal-organic frameworks, in *Metal-Organic Frameworks for Chemical Reactions*, (Elsevier, 2021), pp. 295–330
54. X. Wang, Z. Lin, Robust, hydrophobic anti-corrosion coating prepared by PDMS modified epoxy composite with graphite nanoplatelets/nano-silica hybrid nanofillers. Surf. Coat. Technol. **421**, 127440 (2021)
55. G.M. Nair, T. Sajini, B. Mathew, Advanced green approaches for metal and metal oxide nanoparticles synthesis and their environmental applications. Talanta Open **5**, 100080 (2021)
56. S. Kango, S. Kalia, A. Celli, J. Njuguna, Y. Habibi, R. Kumar, Surface modification of inorganic nanoparticles for development of organic–inorganic nanocomposites—A review. Prog. Polym. Sci. **38**(8), 1232–1261 (2013)
57. A.M. El Saeed, M. Abd El-Fattah, A.M. Azzam, Synthesis of ZnO nanoparticles and studying its influence on the antimicrobial, anticorrosion and mechanical behavior of polyurethane composite for surface coating. Dyes Pigments **121**, 282–289 (2015)
58. X. Xiao, L. Miao, G. Xu, L. Lu, Z. Su, N. Wang, S. Tanemura, A facile process to prepare copper oxide thin films as solar selective absorbers. Appl. Surf. Sci. **257**(24), 10729–10736 (2011)
59. R. Albatici, F. Passerini, A.M. Tonelli, S. Gialanella, Assessment of the thermal emissivity value of building materials using an infrared thermovision technique emissometer. Energ. Buildings **66**, 33–40 (2013)

60. A.H. Jayatissa, K. Guo, A.C. Jayasuriya, Fabrication of cuprous and cupric oxide thin films by heat treatment. Appl. Surf. Sci. **255**(23), 9474–9479 (2009)
61. J. Karthikeyan, The advantages and disadvantages of the cold spray coating process, in *The Cold Spray Materials Deposition Process*, (Woodhead Publishing, 2007), pp. 62–71
62. W.J. Stepniowski, W.Z. Misiolek, Review of fabrication methods, physical properties, and applications of nanostructured copper oxides formed via electrochemical oxidation. Nanomaterials **8**(6), 379 (2018)
63. F. Jiang, W. Zhao, Y. Wu, J. Dong, K. Zhou, G. Lu, J. Pu, Anti-corrosion behaviors of epoxy composite coatings enhanced via graphene oxide with different aspect ratios. Prog. Org. Coat. **127**, 70–79 (2019)
64. D. Okanigbe, P. Olawale, A. Popoola, A. Abraham, A. Michael, K. Andrei, Centrifugal separation experimentation and optimum predictive model development for copper recovery from waste copper smelter dust. Cogent Eng. **5**(1), 1551175 (2018)
65. S. Saha, J. Khan, T. Knight, T. Farouk, A global model for predicting vacuum drying of used nuclear fuel assemblies. Nucl. Technol. **208**(3), 414–427 (2022)
66. A. Pasha, S. Khasim, A.A.A. Darwish, T.A. Hamdalla, S.A. Al-Ghamdi, High performance organic coatings of polypyrrole embedded with manganese iron oxide nanoparticles for corrosion protection of conductive copper surface. J. Inorg. Organomet. Polym. Mater. **32**(2), 499–512 (2022)
67. C. Huang, X. Qian, R. Yang, Thermal conductivity of polymers and polymer nanocomposites. Mater. Sci. Eng. R Rep. **132**, 1–22 (2018)
68. F. Jiang, S. Cui, C. Rungnim, N. Song, L. Shi, P. Ding, Control of a dual-cross-linked boron nitride framework and the optimized design of the thermal conductive network for its thermo-responsive polymeric composites. Chem. Mater. **31**(18), 7686–7695 (2019)
69. X. Fu, Z. Ji, W. Lin, Y. Yu, T. Wu, The advancement of neutron shielding materials for the storage of spent nuclear fuel. Sci. Technol. Nucl. Install. **2021**, 5541047 (2021)
70. C.K. Wilson, The 1996 IAEA regulations for the safe transport of radioactive materials—The transport of fissile material. Int. J. Radioact. Mater. Transp. **8**(2), 127–132 (1997)
71. Y. Song, F. Jiang, N. Song, L. Shi, P. Ding, Multilayered structural design of flexible films for smart thermal management. Compos. A: Appl. Sci. Manuf. **141**, 106222 (2021)
72. Z. Zhu, C. Li, E. Songfeng, L. Xie, R. Geng, C.T. Lin, L. Li, Y. Yao, Enhanced thermal conductivity of polyurethane composites via engineering small/large sizes interconnected boron nitride nanosheets. Compos. Sci. Technol. **170**, 93–100 (2019)
73. J.S. George, J.K. Paduvilan, N. Salim, J. Sunarso, N. Kalarikkal, N. Hameed, S. Thomas, Advances and future outlook in epoxy/graphene composites for anticorrosive applications. Prog. Org. Coat. **162**, 106571 (2022)
74. J. Zhang, W. Zhang, L. Wei, L. Pu, J. Liu, H. Liu, Y. Li, J. Fan, T. Ding, Z. Guo, Alternating multilayer structural epoxy composite coating for corrosion protection of steel. Macromol. Mater. Eng. **304**(12), 1900374 (2019)
75. N. Keshmiri, P. Najmi, M. Ramezanzadeh, B. Ramezanzadeh, Designing an eco-friendly lanthanide-based metal organic framework (MOF) assembled graphene-oxide with superior active anti-corrosion performance in epoxy composite. J. Clean. Prod. **319**, 128732 (2021)
76. Z. Yu, L. Lv, Y. Ma, H. Di, Y. He, Covalent modification of graphene oxide by metronidazole for reinforced anti-corrosion properties of epoxy coatings. RSC Adv. **6**(22), 18217–18226 (2016)
77. M. Conradi, A. Kocijan, D. Kek-Merl, M. Zorko, I. Verpoest, Mechanical and anticorrosion properties of nanosilica-filled epoxy-resin composite coatings. Appl. Surf. Sci. **292**, 432–437 (2014)
78. C.Y. Ge, X.G. Yang, B.R. Hou, Synthesis of polyaniline nanofiber and anticorrosion property of polyaniline–epoxy composite coating for Q235 steel. J. Coat. Technol. Res. **9**(1), 59–69 (2012)
79. P. Ghahremani, A.H. Mostafatabar, G. Bahlakeh, B. Ramezanzadeh, Rational design of a novel multi-functional carbon-based nano-carrier based on multi-walled-CNT-oxide/polydo-

pamine/chitosan for epoxy composite with robust pH-sensitive active anti-corrosion properties. Carbon **189**, 113–141 (2022)
80. M. Motamedi, M. Ramezanzadeh, B. Ramezanzadeh, M. Mahdavian, One-pot synthesis and construction of a high performance metal–organic structured nano pigment based on nanoceria decorated cerium (III)-imidazole network (NC/CIN) for effective epoxy composite coating anti-corrosion and thermo-mechanical properties improvement. Chem. Eng. J. **382**, 122820 (2020)
81. R. Hsissou, O. Dagdag, M. Berradi, M. El Bouchti, M. Assouag, A. Elharfi, Development rheological and anti-corrosion property of epoxy polymer and its composite. Heliyon **5**(11), e02789 (2019)
82. S.M. Lashgari, H. Yari, M. Mahdavian, B. Ramezanzadeh, G. Bahlakeh, M. Ramezanzadeh, Application of nanoporous cobalt-based ZIF-67 metal-organic framework (MOF) for construction of an epoxy-composite coating with superior anti-corrosion properties. Corros. Sci. **178**, 109099 (2021)
83. S. Chhetri, P. Samanta, N.C. Murmu, T. Kuila, Anticorrosion properties of epoxy composite coating reinforced by molybdate-intercalated functionalized layered double hydroxide. J. Compos. Sci. **3**(1), 11 (2019)
84. K. Cao, Z. Yu, D. Yin, Preparation of Ce-MOF@ TEOS to enhance the anti-corrosion properties of epoxy coatings. Prog. Org. Coat. **135**, 613–621 (2019)
85. Y. Wu, J. Yu, W. Zhao, C. Wang, B. Wu, G. Lu, Investigating the anti-corrosion behaviors of the waterborne epoxy composite coatings with barrier and inhibition roles on mild steel. Prog. Org. Coat. **133**, 8–18 (2019)
86. C. Yu, J. Zhang, Z. Li, W. Tian, L. Wang, J. Luo, Q. Li, X. Fan, Y. Yao, Enhanced through-plane thermal conductivity of boron nitride/epoxy composites. Compos. A: Appl. Sci. Manuf. **98**, 25–31 (2017)
87. F. Jiang, S. Cui, N. Song, L. Shi, P. Ding, Hydrogen bond-regulated boron nitride network structures for improved thermal conductive property of polyamide-imide composites. ACS Appl. Mater. Interfaces **10**(19), 16812–16821 (2018)
88. X.J. Zha, J. Yang, J.H. Pu, C.P. Feng, L. Bai, R.Y. Bao, Z.Y. Liu, M.B. Yang, W. Yang, Enhanced thermal conductivity and balanced mechanical performance of PP/BN composites with 1 vol% finely dispersed MWCNTs assisted by OBC. Adv. Mater. Interfaces **6**(9), 1900081 (2019)
89. J. Gu, K. Ruan, Breaking through bottlenecks for thermally conductive polymer composites: A perspective for intrinsic thermal conductivity, interfacial thermal resistance and theoretics. Nanomicro Lett. **13**(1), 1–9 (2021)
90. A. Aparna, A.S. Sethulekshmi, J.S. Jayan, A. Saritha, K. Joseph, Recent advances in boron nitride based hybrid polymer nanocomposites. Macromol. Mater. Eng. **306**(11), 2100429 (2021)
91. D. Zou, X. Huang, Y. Zhu, J. Chen, P. Jiang, Boron nitride nanosheets endow the traditional dielectric polymer composites with advanced thermal management capability. Compos. Sci. Technol. **177**, 88–95 (2019)
92. Y. Han, X. Shi, X. Yang, Y. Guo, J. Zhang, J. Kong, J. Gu, Enhanced thermal conductivities of epoxy nanocomposites via incorporating in-situ fabricated hetero-structured SiC-BNNS fillers. Compos. Sci. Technol. **187**, 107944 (2020)
93. F. Kargar, Z. Barani, R. Salgado, B. Debnath, J.S. Lewis, E. Aytan, R.K. Lake, A.A. Balandin, Thermal percolation threshold and thermal properties of composites with high loading of graphene and boron nitride fillers. ACS Appl. Mater. Interfaces **10**(43), 37555–37565 (2018)
94. R. Künzel, E. Okuno, Effects of the particle sizes and concentrations on the X-ray absorption by CuO compounds. Appl. Radiat. Isot. **70**(4), 781–784 (2012)
95. M.E. Mahmoud, R.M. El-Sharkawy, E.A. Allam, R. Elsaman, A. El-Taher, Fabrication and characterization of phosphotungstic acid-copper oxide nanoparticles-plastic waste nanocomposites for enhanced radiation-shielding. J. Alloys Compd. **803**, 768–777 (2019)

96. H.M. Abd El-Lateef, M. Gouda, Novel nanocomposites of nickel and copper oxide nanoparticles embedded in a melamine framework containing cellulose nanocrystals: Material features and corrosion protection applications. J. Mol. Liq. **342**, 116960 (2021)
97. D. Hassan, A. Hashim, Structural and optical properties of (polystyrene–copper oxide) nanocomposites for biological applications. J. Bionanosci. **12**(3), 341–345 (2018)
98. A.T. Sunny, M. Mozetic, G. Primc, S. Mathew, S. Thomas, Tunable morphology and hydrophilicity to epoxy resin from copper oxide nanoparticles. Compos. Sci. Technol. **146**, 34–41 (2017)
99. A.T. Sunny, R. Adhikari, S. Mathew, S. Thomas, Copper oxide nanoparticles in an epoxy network: Microstructure, chain confinement and mechanical behaviour. Phys. Chem. Chem. Phys. **18**(29), 19655–19667 (2016)
100. V.B. Rajendren, K. Subramani, *Studies on Thermal Conductivity and Thermal Stability of Cu-CNT Composite Powder Filled Epoxy Composites Using a Novel Approach for Sophisticated Thermal Management Applications* (2021)
101. K.A. Jasim, R.N. Fadhil, A.H. Shaban, H.I. Jaafar, B.K. Maiyaly, S.H. Aleabi, E.M. Salman, The effects of copper additives on the glass transition temperature and hardness for epoxy resin. Prog. Ind. Ecol. Int. J. **13**(2), 163–172 (2019)
102. M.H. Nazari, Y. Zhang, A. Mahmoodi, G. Xu, J. Yu, J. Wu, X. Shi, Nanocomposite organic coatings for corrosion protection of metals: A review of recent advances. Prog. Org. Coat. **162**, 106573 (2022)
103. H. Zhang, J. Cao, L. Sun, F. Kong, J. Tang, X. Zhao, Y. Tang, Y. Zuo, Comparative study on the degradation of two self-polishing antifouling coating systems with copper-based antifouling agents. Coatings **12**(8), 1156 (2022)
104. M.M. El-Masry, N.G. Imam, A comparative study between Ag-CuO/epoxy and Mg-CuO/epoxy hybrid nanocomposites: Impressive electrical, mechanical and thermal properties. J. Mater. Res. Technol. **18**, 1784–1801 (2022)
105. Y. Agari, T. Uno, Estimation on thermal conductivities of filled polymers. J. Appl. Polym. Sci. **32**(7), 5705–5712 (1986)
106. A. Agrawal, A. Satapathy, Development of a heat conduction model and investigation on thermal conductivity enhancement of AlN/epoxy composites. Procedia Eng. **51**, 573–578 (2013)
107. D.O. Okanigbe, Production of copper and copper oxide nano-particles from leach solution of low grade copper smelter dust. Dissertation, Tshwane University of Technology, 2019